Multiscale anisotropic fluctuations in sheared turbulence with multiple states

Kartik P. Iyer,[1,2,*] Fabio Bonaccorso,[1] Luca Biferale,[1] and Federico Toschi[3,4]

[1]*Department of Physics and INFN, University of Rome Tor Vergata, 00133 Rome, Italy*
[2]*Department of Mechanical Engineering, New York University, New York 11201, USA*
[3]*Department of Physics, Eindhoven University of Technology, 5600 MB Eindhoven, Netherlands*
[4]*IAC, CNR, 00185 Rome, Italy*

We use high-resolution direct numerical simulations to study the anisotropic contents of a turbulent, statistically homogeneous flow with random transitions among multiple energy containing states. We decompose the velocity correlation functions on different sectors of the three-dimensional group of rotations, SO(3), using a high-precision quadrature. Scaling properties of anisotropic components of longitudinal and transverse velocity fluctuations are accurately measured at changing Reynolds numbers. We show that independently of the anisotropic content of the energy containing eddies, small-scale turbulent fluctuations recover isotropy and universality faster than previously reported in experimental and numerical studies. The discrepancies are ascribed to the presence of highly anisotropic contributions that have either been neglected or measured with less accuracy in the foregoing works. Furthermore, the anomalous anisotropic scaling exponents are devoid of any sign of saturation with increasing order. Our study paves the way to systematically assess persistence of anisotropy in high-Reynolds-number flows.

The notion that all turbulent flows attain *universal* properties at small scales, regardless of the macroscopic details, has been an enduring and yet unproved concept in turbulence research [1–3]. The energy containing scales in many flows such as shear, rotation, natural convection, thick layers, atmospheric boundary layer, and magnetohydrodynamic flows are all strongly affected by anisotropic (and nonhomogeneous) effects of the extrinsic stirring and boundary conditions, resulting in seemingly different flow configurations [4–13]. As such, anisotropic fluctuations are always connected to some degree of nonuniversality, i.e., dependence on the empirical setup. Can we disentangle anisotropic from isotropic statistical contributions? Are there any universal facets of turbulence? How does the relative importance of anisotropic and isotropic fluctuations vary with turbulence intensity? These are the questions we attempt to address.

On the one hand, all phenomenological turbulence theories point toward a return-to-isotropy, at small enough scales [1–3]. On the other hand, measurements of anisotropic contributions as functions of scale separation have revealed persistent small-scale anisotropy in hydrodynamical turbulence [14–18], magnetohydrodynamics [19,20], and passive scalar mixing [21,22]. The persistence of anisotropy as reported in Refs. [16,17,21] was later reconciled with the postulate of local isotropy as an effect of the existence of anomalous scaling in both isotropic and anisotropic correlation functions [22,23].

In this Rapid Communication we investigate the return to isotropy vs persistence of anisotropy, using direct numerical simulations (DNS) of turbulent flows subject to large-scale shear at high Reynolds numbers $\mathrm{Re} \equiv u'r_f/\nu$, where r_f denotes the typical forcing scale, u' is the root-mean-square velocity fluctuation, and ν is the viscosity. We use an *exact* decomposition of multipoint turbulent correlation functions in the eigenbasis of the SO(3) group of rotations, which is the only systematic method to disentangle isotropic from anisotropic contributions and to further

---

*kartik.iyer@nyu.edu
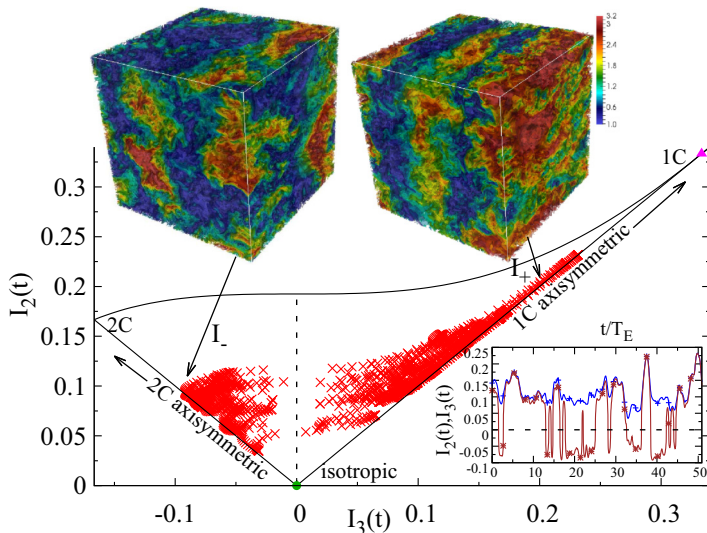
FIG. 1. Evolution of I_3 and I_2 in the Lumley triangle ($\times$) for the 2048^3 RKF. The laminar state given by the forcing configuration is shown by ($\blacktriangle$). The inset shows steady-state evolution of I_2 ($+$) and I_3 ($*$) as functions of t/T_E. The reference line at zero is the isotropic state. Typical isocontours of the velocity magnitude in the 1C (I_+) and 2C (I_-) regions are also shown.

distinguish among different anisotropic turbulent fluctuations. However, the utility of the SO(3) decomposition has largely been impeded by practical difficulties in both experiments and simulations. High-Reynolds-number experiments are beset with limitations on the set of directions that can be probed in three-dimensional (3D) space and consequently resort to *ad hoc* curve fits to separate isotropic from anisotropic scaling properties [24]. Similarly, simulations have until now managed to perform the SO(3) decomposition at low Reynolds numbers only [22], due to computational bottlenecks (see the Supplemental Material [25] for an estimate). Consequently, until now results concerning the multiscale statistical properties of anisotropic fluctuations have been characterized by considerable scatter, thus calling into question their universal nature and in some instances even jeopardizing the fundamental postulate of small-scale isotropy [18].

The main features of this work are the following. First, we have achieved sufficiently high Reynolds numbers for a paradigmatic homogeneous shear configuration obtained from a random Kolmogorov flow (RKF). Second, we have adopted a highly accurate Lebedev quadrature [26,27] for expanding the correlation functions in the irreducible representations of the SO(3) symmetry group. On an N^3 grid, our SO(3) algorithm reduces the computational complexity from $\sim O(N^6)$ to $\sim O(N^3 \log N)$, thus expanding the range of problems where the SO(3) decomposition can be viable (see the Supplemental Material [25] and Refs. [28,29] for details regarding computational intensity).

We discover that the flow evolution reveals unexpected bimodal statistics of the energy containing scale, characterized by chaotic oscillations between two states I_+ and I_-, corresponding to predominantly one-component (1C) and two-component (2C) axisymmetric macrostates (see 3D rendering in Fig. 1), respectively. We exploit the existence of the two macrostates in assessing universality as a function of the large-scale flow configurations. The main results are the following. (i) By going to smaller and smaller scales, isotropy is recovered faster than previously thought. We argue that this is due to the existence of nonvanishing anisotropic contributions from the $j = 4$ sector (see below) discarded or incorrectly measured in previous works [18,30,31]. (ii) We show that the anisotropic fluctuations of longitudinal and transverse velocity increments scale similarly. We confirm the theoretical expectation that all nonuniversal contributions are hidden in the power-law prefactors, sector by sector in the SO(3) decomposition of the velocity correlations.

TABLE I. Listed are the following DNS parameters: Taylor scale Reynolds number $R_\lambda = \sqrt{20\,\mathrm{Re}/3}$, resolution N^3, $k_{\max}\eta = N\eta/3$ [where $\eta = (\nu^3/\epsilon)^{1/4}$ is the Kolmogorov length scale with ϵ the mean dissipation], the forced wave vectors $\mathbf{k}_1$ and $\mathbf{k}_2$, the nondimensional shear rate FT_E/u' (where F is the anisotropic forcing amplitude), and the length of the stationary-state simulation in multiples of large-eddy turnover time T_E, T_{tot}/T_E.

R_λ	N	$k_{\max}\eta$	$\mathbf{k}_1$	$\mathbf{k}_2$	FT_E/u'	T_{tot}/T_E
290	1024	1.94	$\pm(2,0,0)$	$\pm(1,0,0)$	0.48	118
450	2048	1.92	$\pm(2,0,0)$	$\pm(1,0,0)$	0.45	50

(iii) The anisotropic scaling properties, contrary to previous expectations based on low-Reynolds-number calculations, do not saturate at higher orders and are universal and Reynolds independent at least up to the values investigated here.

We study the RKF [31] by evolving the 3D incompressible Navier-Stokes equations in a triperiodic domain,

$$\partial\mathbf{u}/\partial t + \mathbf{u}\cdot\nabla\mathbf{u} = -\nabla p/\rho + \nu\nabla^2\mathbf{u} + \mathbf{f}, \tag{1}$$

where p is the pressure and ρ is the constant density. An anisotropic and statistically stationary state is attained by forcing only two wave numbers (see Table I) in the y direction, $f_y(\mathbf{x},t) = F[\tilde{f}_y(\mathbf{k}_1,t)e^{i\mathbf{k}_1\cdot\mathbf{x}} + \tilde{f}_y(\mathbf{k}_2,t)e^{i\mathbf{k}_2\cdot\mathbf{x}}]$, where F is a constant amplitude and the Fourier coefficients $\tilde{f}_y(\mathbf{k}_{1,2},t)$ follow independent divergence-free Ornstein-Uhlenbeck processes [32]. At variance with the standard nonhomogeneous Kolmogorov flow [33], we recover translationally invariant statistics by averaging the random forcing phases over multiple large-eddy turnover times $T_E \equiv r_f/u'$. To quantify the anisotropy in the energy containing scales we examine the temporal evolution of the two invariants $I_2(t) = (b_{ij}b_{ji}/6)^{1/2}$ and $I_3(t) = (b_{ij}b_{jk}b_{ki}/6)^{1/3}$ of the Reynolds stress $b_{ij} = (\langle u_i u_j\rangle/\langle u_k u_k\rangle) - \delta_{ij}/3$ [34]. Figure 1 shows I_2 plotted against I_3 at different time instants, in the Lumley triangle [35]. Surprisingly enough, despite the high Reynolds number, the dynamics is attracted by two different anisotropic axisymmetric states I_+ and I_-, where $I_3 > 0$ and $I_3 < 0$, respectively. The isocontours of the kinetic energy magnitude reveal a stark contrast in the large-scale structures between the 1C and the 2C macrostates (see Fig. 1). The transition between I_+ and I_- occurs suddenly during the time evolution, as shown in the inset of the same figure by the temporal evolution of the two invariants. Notice that the large-scale configurations always avoid the isotropic $I_2 = I_3 = 0$ state. The oscillations in the Reynolds stress suggest the existence of multiple turbulent states akin to those found in Taylor-Couette and von Kármán swirling flows [36–38]. Here, to assess the degree of small-scale universality at changing the large-scale anisotropy, we will show results conditioned on the sign of I_3.

The longitudinal and transverse velocity increments are defined as $\delta u_L(\mathbf{x},\mathbf{r}) \equiv \delta\mathbf{u}(\mathbf{x},\mathbf{r})\cdot\hat{\mathbf{r}}$ and $\delta\mathbf{u}_T(\mathbf{x},\mathbf{r}) \equiv \delta\mathbf{u}(\mathbf{x},\mathbf{r}) - \delta u_L(\mathbf{x},\mathbf{r})\hat{\mathbf{r}}$, respectively, where $\delta\mathbf{u}(\mathbf{x},\mathbf{r}) \equiv \mathbf{u}(\mathbf{x}+\mathbf{r}) - \mathbf{u}(\mathbf{x})$ is the two-point velocity difference at separation vector $\mathbf{r}$ and $\hat{\mathbf{r}}$ is the unit vector along $\mathbf{r}$. The pth-order longitudinal structure function (LSF) and transverse structure function (TSF) are, respectively,

$$S^{(p,L)}(\mathbf{r}) \equiv \langle[\delta u_L(\mathbf{x},\mathbf{r})]^p\rangle, \tag{2}$$

$$S^{(p,T)}(\mathbf{r}) \equiv \langle[\delta\mathbf{u}_T(\mathbf{x},\mathbf{r})\cdot\delta\mathbf{u}_T(\mathbf{x},\mathbf{r})]^{p/2}\rangle, \tag{3}$$

where $\langle\cdot\rangle$ denotes space and time averages. Since $S^{(p,L)}(\mathbf{r})$ are scalar functions of a vector argument, they can be expanded in spherical harmonics $Y_{jm}(\hat{\mathbf{r}})$ [39] as

$$S^{(p,L)}(\mathbf{r}) = \sum_{j=0}^{\infty}\sum_{m=-j}^{m=+j} S_{j,m}^{(p,L)}(r)Y_{jm}(\hat{\mathbf{r}}). \tag{4}$$
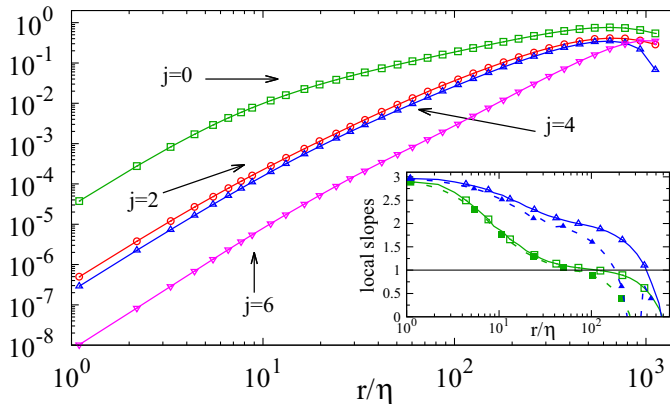
FIG. 2. A log-log plot of $|S_{j,m}^{(3,L)}|$ vs r for different (j,m) sectors at $R_\lambda = 450$. Symbols correspond to sectors $(0,0)$ ($\square$), $(2,0)$ ($\circ$), $(4,4)$ ($\triangle$), and $(6,6)$ ($\triangledown$), respectively. The inset shows the corresponding logarithmic local slopes for sectors $(0,0)$ and $(4,4)$ at $R_\lambda = 300$ (closed symbols) and $R_\lambda = 450$ (open symbols). The horizontal line at 1.0 is the exact result for sector $(0,0)$ [41].

The index j labels the different degrees of anisotropy, while the dependence on m distinguishes different degrees of freedom within a given anisotropic sector. The TSF can be expanded similarly via the corresponding projections $S_{j,m}^{(p,T)}$. The projection on the $j = 0$ sector corresponds to the isotropic case, the only one that will survive if the external forcing is invariant under rotation. Theoretical speculations suggest that at high enough Re and for small enough scales $r \ll r_f$, a foliation of the physics in different j sectors occurs, characterized by different power-law scaling [22,40],

$$S_{j,m}^{(p,L)}(r) = \Lambda_{j,m}^{(p,L)} \left(\frac{r}{r_f} \right)^{\xi_j^L(p)},$$

$$S_{j,m}^{(p,T)}(r) = \Lambda_{j,m}^{(p,T)} \left(\frac{r}{r_f} \right)^{\xi_j^T(p)}. \tag{5}$$

All questions can then be translated in terms of the above-defined quantities. Recovery of isotropy (universality) implies that a strict hierarchy exists among the isotropic and anisotropic exponents, $\xi_0^L(p) < \xi_{j>0}^L(p)$. The rate of recovery is measured by the gap between the exponents of the same order: The smaller the gap, the more slowly the anisotropic contributions decay. Theoretical considerations suggest that the exponents $\xi_j^L(p)$ and $\xi_j^T(p)$ are universal, i.e., independent of the large-scale configuration. The prefactors $\Lambda_{j,m}^{(p,L)}$ and $\Lambda_{j,m}^{(p,T)}$ must be nonuniversal, being determined by the matching for $r \sim r_f$. The exact expansion (4) together with scaling assumption (5) implies that in the presence of anisotropy, multiple power laws are present in the undecomposed correlations such as $S^{(p,L)}(\mathbf{r})$ and hence nontrivial subleading terms can contaminate their scaling behavior. Conversely, the projected components $S_{j,m}^{(p,L)}$ must show a pure power-law behavior. In Fig. 2 we assess the rate of recovery of isotropy by plotting the magnitudes $|S_{j,m}^{(p,L)}(r)|$ for $p = 3$, up to $j = 6$ [we omit those (j,m) sectors that have negligible intensity or that have similar scaling properties]. All projections exhibit a clear power-law behavior. The isotropic projection scales quasilinearly in the scale range $44 \leqslant r/\eta \leqslant 350$, as it does in an isotropic flow, due to the 4/5 law [41–43]. All sectors have comparable magnitude at the forcing scale, confirming the strong anisotropy of the energy containing scales. In contrast, the anisotropic projections become more and more subleading with decreasing r. The quality of the scaling properties are shown in the inset of Fig. 2, where we compare the logarithmic derivatives of $j = 0$ and $j = 4$ at two different Reynolds numbers. Similar plots are obtained for other moments and for transverse increments. It is important to stress
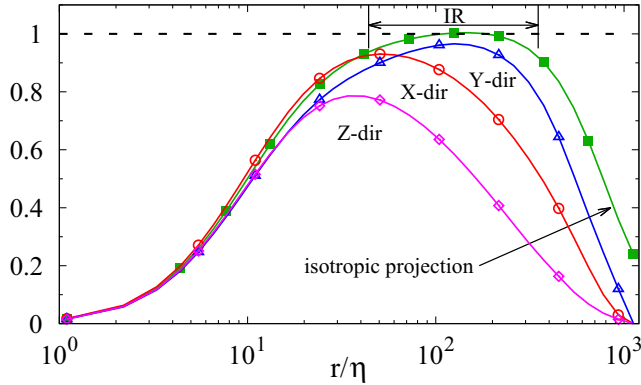
FIG. 3. A lin-log plot of the undecomposed compensated structure function $-5S^{(3,L)}(\mathbf{r})/4r\epsilon$ at $R_\lambda = 450$ along the Cartesian directions $\hat{x}$ ($\circ$), $\hat{y}$ ($\triangle$), and $\hat{z}$ ($\diamond$). The corresponding projection on the isotropic sector $-5S^{(3,L)}_{(0,0)}(r)Y_{00}/4r\epsilon$ is given by ($\blacksquare$). The inertial range (IR) is taken as that range within 5% of the exact IR result, shown by the dashed line at unity.

that the anisotropic projections shown in Fig. 2 display a quality of scaling never achieved before concerning both statistical accuracy and extension of the inertial range of scales. An extremely high numerical and statistical accuracy is required to disentangle fluctuations that differ up to four orders of magnitude (compare sectors $j = 6$ and $j = 0$ at the smallest r). These results have been possible due to the highly accurate quadrature that has been used for the SO(3) decomposition (see the Supplemental Material [25] for details concerning accuracy and convergence of the Lebedev quadrature).

Despite anisotropies being subleading at the small scales, their cumulative effects are important and strongly influence scaling laws if not properly decomposed. This is shown in Fig. 3, which compares the undecomposed third-order LSF along the three Cartesian directions along with the projection on the isotropic sector, all compensated with the exact isotropic 4/5 linear behavior, $-4/5\epsilon r$. The undecomposed correlations do not compensate well and depend on the chosen direction. In contrast, the isotropic sector confirms the Kolmogorov plateau [41] on a wide range of scales [44].

To assess universality of the scaling properties sector by sector, we show in Fig. 4 that both $S^{(p,L)}_{j,m}$ [Fig. 4(a)] and $S^{(p,T)}_{j,m}$ [Fig. 4(b)] scale similarly when conditioned on I_+ or I_- events. Using
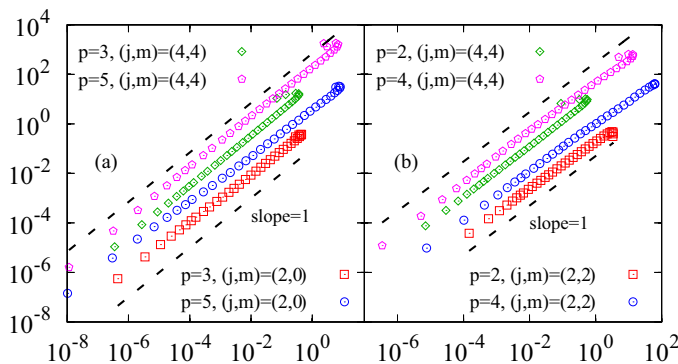
FIG. 4. (a) A log-log plot of $S^{(p,L)}_{j,m}|_{I_+}$ vs $S^{(p,L)}_{j,m}|_{I_-}$ at various orders p and sectors (j,m). (b) Same as (a) but for the transverse structure functions. Universality with respect to large-scale conditioning corresponds to slope 1 as shown by the dashed straight lines. For clarity, curves are offset upward.
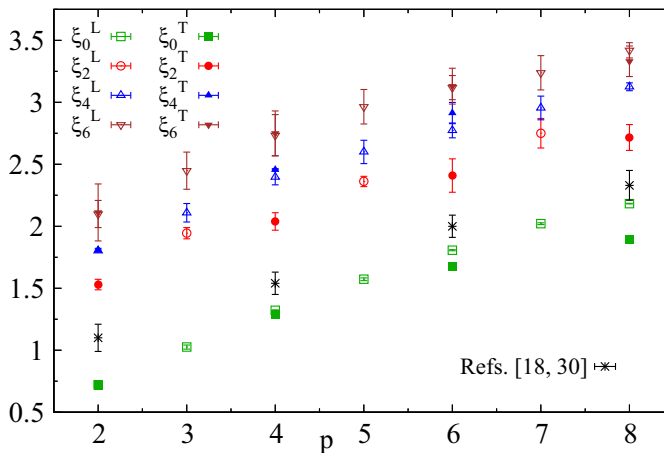
FIG. 5. Summary of scaling exponents of $S_{j,m}^{(p,L)}$ (open symbols) and $S_{j,m}^{(p,T)}$ (closed symbols) vs order p for sectors $j \leqslant 6$. Error bars indicate 95% confidence intervals. Data from experiments for $j = 2$ ($*$) are given for comparison [18,30].

a least-squares fit we find that the relative scaling exponents for all curves is ~ 1 within 5%. This supports the foliation argument that the scaling exponents, sectorwise, are immune to anisotropic large-scale effects and hence are universal.

The summary for all scaling exponents of different LSF and TSF projections on the different sectors are plotted for various orders in Fig. 5. A few final comments are in order. (i) Both $\xi_j^L(p)$ and $\xi_j^T(p)$ have similar values, except for small deviations at orders $p \geqslant 6$ in the $j = 0$ sector (see Refs. [45–47] for a discussion on the Reynolds-number dependence of the isotropic exponents). (ii) At any given order p, a finite gap exists between isotropic and anisotropic exponents, indicating a strict asymptotic recovery of isotropy for the whole probability distribution function. (iii) For any j, the scaling exponents do not scale linearly in p, contrary to the dimensional prediction $\xi_{j,\dim}(p) = (p + j)/3$ proposed in Ref. [48], indicating that anomalous scaling is also present in $j > 0$ sectors. Importantly enough, the SO(3) scheme using a high-order Lebedev rule [49,50] enables us to clean the previously reported results. For example, in contrast to Ref. [31], we find that the exponents in any given anisotropic sector increase with order p with no apparent saturation. We contend that the saturation observed in Ref. [31] is due to spurious effects induced by combination of poor accuracy in the SO(3) expansion and potential contamination by hyperviscous effects. In Fig. 5 we also report results for the $j = 2$ sector from the few prior experiments [18,30]. In experiments, it is difficult to perform measurements along a sufficiently large number of directions to adequately resolve the anisotropic fluctuations on the 2-sphere, in contrast $\sim O(1000)$ different directions were used in this work. As a result, experiments must resort to a fit for the entire right-hand side of Eq. (4) using data along a few directions only. In order to reduce the number of fitting parameters, the sum on all sectors is typically cut at $j = 2$, something that is clearly not enough in view of the results shown in Fig. 2. Indeed, we find that sector $j = 4$ is almost as energetic as $j = 2$, with a very similar scaling exponent, i.e., the $j = 4$ contribution is as important as $j = 2$, at almost all scales. Figure 5 shows that the results from our exact decomposition clearly differ from that of Refs. [18,30], wherein sectors $j \geqslant 4$ are neglected. In the presence of many anisotropic sectors, obtaining scaling exponents by assuming that only the lowest anisotropic sector is dominant can strongly affect the measured rate of return owing to spurious cancellations. Only the exact SO(3) expansion allows the measurement of $\xi_j(p)$, devoid of contamination from sectors $j' \neq j$, thus yielding a true gauge of the rate of return at a given order p. It remains to be clarified if in the homogeneous shear case

analyzed in Refs. [17,18] the scaling properties of high-order sectors $j \geqslant 4$ are also as important as in the RKF.

In conclusion, we have used an efficient algorithm for the SO(3) decomposition, to study anisotropy in high-Reynolds-number Kolmogorov flows. We have found that the RKF develops a two-state attractor characterized by very different anisotropic large-scale contents. We have shown that the scaling exponents in RKF are immune to different large-scale effects and hence are universal. The magnitude of the anisotropic exponents indicates that isotropy is recovered at a faster rate than previously thought. Nevertheless, projection on the SO(3) is mandatory to detect a clean scaling, since power laws exist only sector by sector. We do not observe saturation of exponents at the higher j sectors, indicating that intense anisotropic fluctuations are dominated by more than one singular structure. Differently from previous observations, we demonstrate that it is mandatory to resolve at least up to sector $j = 4$ to have clean scaling properties, sector by sector. We hope our study will stimulate further theoretical or phenomenological efforts to predict the scaling properties for all j sectors. It will be important to extend this analysis to other turbulent flows, such as those in the presence of rotation, mean shear, and magnetic field, in order to establish, on a firmer basis, the degree of universality. The improvement provided by the fast SO(3) solver opens the possibility to perform such studies.

---

[1] A. N. Kolmogorov, Local structure of turbulence in an incompressible fluid for very large Reynolds numbers, Dokl. Akad. Nauk. SSSR **30**, 299 (1941).

[2] U. Frisch, *Turbulence* (Cambridge University Press, Cambridge, 1995).

[3] S. B. Pope, *Turbulent Flows* (Cambridge University Press, Cambridge, 2000).

[4] B. Dhruva, Y. Tsuji, and K. R. Sreenivasan, Transverse structure functions in high-Reynolds-number turbulence, Phys. Rev. E **56**, R4928 (1997).

[5] F. S. Godeferd and F. Moisy, Structure and dynamics of rotating turbulence: A review of recent experimental and numerical results, ASME Appl. Mech. Rev. **67**, 030802 (2015).

[6] H. Xia, D. Byrne, G. Falkovich, and M. Shats, Upscale energy transfer in thick turbulent fluid layers, Nat. Phys. **7**, 321 (2011).

[7] B. Saint-Michel, B. Dubrulle, L. Marié, F. Ravelet, and F. Daviaud, Evidence for Forcing-Dependent Steady States in a Turbulent Swirling Flow, Phys. Rev. Lett. **111**, 234502 (2013).

[8] P. Gualtieri, F. Picano, G. Sardina, and C. M. Casciola, Clustering and turbulence modulation in particle-laden shear flows, J. Fluid Mech. **715**, 134 (2013).

[9] C. Cambon, L. Danaila, F. S. Godeferd, and J. F. Scott, Third-order statistics and the dynamics of strongly anisotropic turbulent flows, J. Turb. **14**, 121 (2013).

[10] K. McCaffrey, B. Fox-Kemper, P. E. Hamlington, and J. Thomson, Characterization of turbulence anisotropy, coherence, and intermittency at a prospective tidal energy site: Observational data analysis, Renew. Energy. **76**, 441 (2015).

[11] G. C. Murphy and M. E. Pessah, On the anisotropic nature of MRI-driven turbulence in astrophysical disks, Astrophys. J. **802**, 139 (2015).

[12] C. C. Liu, R. T. Cerbus, and P. Chakraborty, Janus Spectra in Two-Dimensional Flows, Phys. Rev. Lett. **117**, 114502 (2016).

[13] S. Sukoriansky and G. Galperin, QNSE theory of turbulence anisotropization and onset of the inverse energy cascade by solid body rotation, J. Fluid Mech. **805**, 384 (2016).

[14] S. Tavoularis and S. Corrsin, Experiments in nearly homogeneous turbulent shear flow with a uniform mean temperature gradient. Part 2. The fine structure, J. Fluid Mech. **104**, 349 (1981).

[15] A. Pumir and B. I. Shraiman, Persistent Small Scale Anisotropy in Homogeneous Shear Flows, Phys. Rev. Lett. **75**, 3114 (1995).

[16] S. Garg and Z. Warhaft, On the small scale structure of simple shear flow, Phys. Fluids **10**, 662 (1998).

[17] X. Shen and Z. Warhaft, The anisotropy of the small scale structure in high Reynolds number ($R_\lambda \sim 1000$) turbulent shear flow, Phys. Fluids **12**, 2976 (2000).

[18] Z. Warhaft and X. Shen, On the higher order mixed structure functions in laboratory shear flow, Phys. Fluids **14**, 2432 (2002).

[19] W. C. Müller, D. Biskamp, and R. Grappin, Statistical anisotropy of magnetohydrodynamic turbulence, Phys. Rev. E **67**, 066302 (2003).

[20] W. D. Watson, D. S. Wiebe, J. C. McKinney, and C. F. Gammie, Anisotropy of magnetohydrodynamic turbulence and the polarized spectra of OH masers, Astrophys. J. **604**, 707 (2004).

[21] Z. Warhaft, Passive scalars in turbulent flows, Annu. Rev. Fluid Mech. **32**, 203 (2000).

[22] L. Biferale and I. Procaccia, Anisotropy in turbulent flows and in turbulent transport, Phys. Rep. **414**, 43 (2005).

[23] L. Biferale and M. Vergassola, Isotropy vs anisotropy in small-scale turbulence, Phys. Fluids **13**, 2139 (2001).

[24] I. Arad, B. Dhruva, S. Kurien, V. S. L'vov, I. Procaccia, and K. R. Sreenivasan, The Extraction of Anisotropic Contributions in Turbulent Flows, Phys. Rev. Lett. **81**, 5330 (1998).

[25] See Supplemental Material at http://link.aps.org/supplemental/10.1103/PhysRevFluids.2.052602 for details.

[26] V. I. Lebedev, Values of the nodes and weights of ninth to seventeenth order Gauss-Markov quadrature formulas invariant under the octahedron group with inversion, USSR Comput. Math. Math. Phys. **15**, 44 (1975).

[27] V. I. Lebedev, Quadratures on a sphere, USSR Comput. Math. Math. Phys. **16**, 10 (1976).

[28] D. Pekurovsky, P3DFFT: A framework for parallel computations of Fourier transforms in three dimensions, SIAM J. Sci. Comput. **34**, C192 (2012).

[29] M. Frigo and S. G. Johnson, The design and implementation of FFTW3, Proc. IEEE **93**, 216 (2005), special issue on program generation, optimization, and platform adaptation, edited by J. M. F. Moura, M. Püschel, J. Dongarra, and D. Padua.

[30] S. Kurien and K. R. Sreenivasan, Anisotropic scaling contributions to high-order structure functions in high-Reynolds-number turbulence, Phys. Rev. E **62**, 2206 (2000).

[31] L. Biferale and F. Toschi, Anisotropic Homogeneous Turbulence: Hierarchy and Intermittency of Scaling Exponents in the Anisotropic Sectors, Phys. Rev. Lett. **86**, 4831 (2001).

[32] L. Biferale, F. Bonaccorso, I. M. Mazzitelli, M. A. T. van Hinsberg, A. S. Lanotte, S. Musacchio, P. Perlekar, and F. Toschi, Coherent Structures and Extreme Events in Rotating Multiphase Turbulent Flows, Phys. Rev. X **6**, 041036 (2016).

[33] V. Borue and S. Orszag, Numerical study of three-dimensional Kolmogorov flow at high Reynolds numbers, J. Fluid Mech. **306**, 293 (1996).

[34] K. S. Choi and J. L. Lumley, The return to isotropy of homogenous turbulence, J. Fluid Mech. **436**, 59 (2001).

[35] J. L. Lumley and G. R. Newman, The return to isotropy of homogenous turbulence, J. Fluid Mech. **82**, 161 (1977).

[36] S. G. Huisman, R. C. A. van der Veen, C. Sun, and D. Lohse, Multiple states in highly turbulent Taylor-Couette flow, Nat. Commun. **5**, 3820 (2014).

[37] B. Saint-Michel, B. Dubrulle, L. Marié, F. Ravelet, and F. Daviaud, Influence of Reynolds number and forcing type in a turbulent von Kármán flow, New J. Phys. **16**, 063037 (2014).

[38] S. Thalabard, B. Saint-Michel, E. Herbert, F. Daviaud, and B. Dubrulle, A statistical mechanics framework for the large-scale structure of turbulent von Kármán flows, New J. Phys. **17**, 063006 (2015).

[39] I. Arad, V. S. L'vov, and I. Procaccia, Correlation functions in isotropic and anisotropic turbulence: The role of the symmetry group, Phys. Rev. E **59**, 6753 (1999).

[40] S. Kurien and K. R. Sreenivasan, in *New Trends in Turbulence: Nouveaux Aspects*, edited by M. Lesieur, A. Yaglom, and F. David, Les Houches—Ecole d'Ete de Physique Theorique Vol. 74 (Springer, Berlin, 2001), p. 53.

[41] A. N. Kolmogorov, Dissipation of energy in locally isotropic turbulence, Dokl. Akad. Nauk SSSR **434**, 16 (1941).

[42] J. Qian, Inertial range and the finite Reynolds number effect of turbulence, Phys. Rev. E **55**, 337 (1997).

[43] T. S. Lundgren, Kolmogorov two-thirds law by matched asymptotic expansion, Phys. Fluids **14**, 638 (2002).

[44] M. A. Taylor, S. Kurien, and G. L. Eyink, Recovering isotropic statistics in turbulence simulations: The Kolmogorov 4/5th law, Phys. Rev. E **68**, 026310 (2003).

[45] S. Chen, K. R. Sreenivasan, M. Nelkin, and N. Cao, Refined Similarity Hypothesis for Transverse Structure Functions in Fluid Turbulence, Phys. Rev. Lett. **79**, 2253 (1997).

[46] R. Benzi, L. Biferale, R. Fisher, D. Q. Lamb, and F. Toschi, Inertial range Eulerian and Lagrangian statistics from numerical simulations of isotropic turbulence, J. Fluid Mech. **653**, 221 (2010).

[47] K. P. Iyer, K. R. Sreenivasan, and P. K. Yeung, Reynolds number scaling of velocity increments in isotropic turbulence, Phys. Rev. E **95**, 021101 (2017).

[48] L. Biferale, I. Daumont, A. Lanotte, and F. Toschi, Anomalous and Dimensional scaling in anisotropic turbulence, Phys. Rev. E **66**, 056306 (2002).

[49] V. I. Lebedev and D. N. Laikov, A quadrature formula for the sphere of the 131st algebraic order of accuracy, Dokl. Math. **59**, 477 (1999).

[50] http://people.sc.fsu.edu/˜jburkardt/f_src/sphere_lebedev_rule/sphere_lebedev_rule.html